J|A|C|S ARTICLES

Published on Web 03/20/2009

Columnar Packing Motifs of Functionalized Perylene Derivatives: Local Molecular Order Despite Long-Range Disorder

Michael Ryan Hansen, Robert Graf, Sivakumar Sekharan, and Daniel Sebastiani*

Max-Planck-Institut für Polymerforschung, Ackermannweg 10, 55128 Mainz, Germany

Received December 8, 2008; E-mail: sebastia@mpip-mainz.mpg.de

Abstract: We elucidate local packing motifs and dynamical order parameters in a perylene tetracarboxydiimide derivative ($C_{8,7}$-PDI), one of the most promising candidates for rationally designed, self-assembling, and self-healing molecular wires. Spectroscopic fingerprints obtained from solid-state NMR spectroscopy are interpreted by means of first-principles calculations and molecular dynamics simulations. The interplay of steric repulsion, H bonding, and $\pi-\pi$ packing effects leads to a specific relative molecular pitch angle of $\sim 35 \pm 10^\circ$ between successive molecules in the stack. Dynamical order parameters, determined from NMR sideband patterns as a measure of molecular motion, yield values of $S \approx 1.0$ in the core of the columnar stack, corresponding to an almost frozen molecular dynamics at ambient temperature. This rigidity is compatible with characteristic intermolecular distances obtained from dipolar couplings between specific hydrogens via double-quantum NMR experiments and further supported by ab initio calculations.

1. Introduction

In the emerging area of molecular electronics, the application of stacks of functionalized molecules as molecular wires has become one of the central goals of current research activities.[1−5] The perspective of using self-assembling, self-healing supramolecular assemblies is extremely promising for nanoscale electronic devices, although the rational design of such self-organizing columnar phases is presently still far from being routine work. While a great deal of research effort is presently being invested in understanding the relationships between chemical functionalization and macroscopic function, there is still relatively little fundamental understanding of the microscopic structure and its dynamical fluctuations on the atomic level.[6,7]

In this work, we shed light on both local structural information and dynamical processes on the atomic and molecular scales for a perylene tetracarboxydiimide derivative, $C_{8,7}$-PDI (see the schematic structure in Figure 1a). A particular feature of PDI derivatives is their variability in terms of morphology, which in turn allows the adjustment of their functionality over a considerable range. In particular, the self-assembly of PDI derivatives can be controlled by extending their core,[8] introducing hydrogen bonding[9] or metal ion coordination,[10] or changing the geometry of the side groups.[11,12] This variability comes along with molecular mobilities that cannot be easily classified into well-established categories, as their ordering characteristics often lie between the crystalline and liquid types. The $C_{8,7}$-PDI molecules self-assemble into columnar phases that have relatively little long-range order, as has recently been revealed by X-ray diffraction studies;[7,8] however, they have sufficient internal stability to support both n- and p-type conductivity and hence might indeed serve as molecular wires.[13−15] The relationship between the supramolecular structure and the charge mobility of columnar perylene tetracarboxydiimide derivatives is presently being investigated in a separate work.[16] The $C_{8,7}$-PDI molecule consists of an aromatic core to which medium-sized alkyl chains are attached; the latter improve the stability of individual stacks and serve as a soft buffer between the stacks. Given a suitable supramolecular arrangement, these stacks allow for one-dimensional electronic charge transport along their centers, making them suitable for advanced

(1) Scheibel, T.; Parthasarathy, R.; Sawicki, G.; Lin, X. M.; Jaeger, H.; Lindquist, S. L. *Proc. Natl. Acad. Sci. U.S.A.* **2003**, *100*, 4527.
(2) Fan, F.-R. F.; Yang, J.; Cai, L.; Price, D. W.; Dirk, S. M.; Kosynkin, D. V.; Yao, Y.; Rawlett, A. M.; Tour, J. M.; Bard, A. J. *J. Am. Chem. Soc.* **2002**, *124*, 5550.
(3) Schenning, A. P. H. J.; Meijer, E. W. *Chem. Commun.* **2005**, 3245.
(4) Wu, J.; Pisula, W.; Müllen, K. *Chem. Rev.* **2007**, *107*, 718.
(5) Zang, L.; Che, Y.; Moore, J. S. *Acc. Chem. Res.* **2008**, *41*, 1596.
(6) Lemaur, V.; da Silva Filho, D. A.; Coropceanu, V.; Lehmann, M.; Geerts, Y.; Piris, J.; Debije, M. G.; van de Craats, A. M.; Senthilkumar, K.; Siebbeles, L. D. A.; Warman, J. M.; Brédas, J.-L.; Cornil, J. *J. Am. Chem. Soc.* **2004**, *126*, 3271.
(7) Marcon, V.; Kirkpatrick, J.; Pisula, W.; Andrienko, D. *Phys. Status Solidi B* **2008**, *245*, 820.
(8) Nolde, F.; Pisula, W.; Müller, S.; Kohl, C.; Müllen, K. *Chem. Mater.* **2006**, *18*, 3715.
(9) Zhang, X.; Chen, Z.; Würthner, F. *J. Am. Chem. Soc.* **2007**, *129*, 4886.
(10) Würthner, F. *Chem. Commun.* **2004**, 1564.
(11) van de Craats, A.; Warman, J.; Schlichting, P.; Rohr, U.; Geerts, Y.; Müllen, K. *Synth. Met.* **1999**, *102*, 1550.
(12) Chen, Z.; Stepanenko, V.; Dehm, V.; Prins, P.; Siebbeles, L. D. A.; Seibt, J.; Marquetand, P.; Engel, V.; Würthner, F. *Chem.—Eur. J.* **2007**, *13*, 436.
(13) Tour, J. M.; Kozaki, M.; Seminario, J. M. *J. Am. Chem. Soc.* **1998**, *120*, 8486.
(14) Lortscher, E.; Elbing, M.; Tschudy, M.; von Hanisch, C.; Weber, H. B.; Mayor, M.; Riel, H. *ChemPhysChem* **2008**, *9*, 2252.
(15) Kirkpatrick, J.; Marcon, V.; Nelson, J.; Kremer, K.; Andrienko, D. *Phys. Rev. Lett.* **2007**, *98*, 227402.
(16) Marcon, V.; Pisula, W.; Dahl, J.; Breiby, D. W.; Kirkpatrick, J.; Patwardhan, S.; Grozema, F.; Andrienko, D. *J. Am. Chem. Soc.* **2009**, submitted for publication.

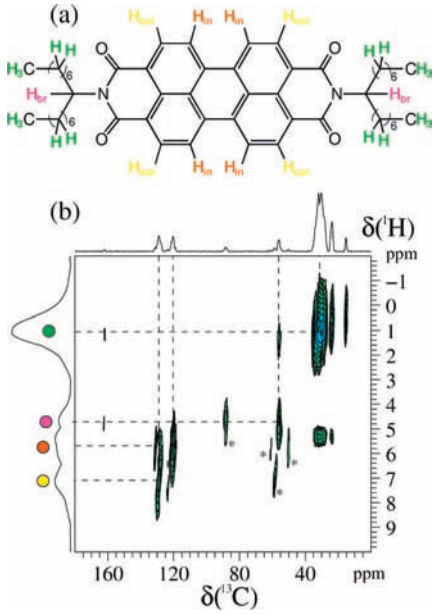

Figure 1. (a) Schematic drawing that illustrates the chemical structure of a single $C_{8,7}$-PDI molecule and shows the nomenclature and color scheme employed for the ^{1}H species throughout this work. (b) 2D contour plot of the ^{13}C{^{1}H} LG-HETCOR correlation experiment for $C_{8,7}$-PDI. Dashed lines indicate the connectivities along with the assignments using the color scheme from (a). The asterisks indicate spinning side bands and an artifact from the transmitter (located in the middle of the 2D spectrum).

nanoscale devices such as organic field-effect transistors and solar cells.[4,17]

Here we combine advanced solid-state magic-angle-spinning (MAS) nuclear magnetic resonance (NMR) experiments with ab initio electronic structure calculations using density functional theory (DFT) and second-order Moller−Plesset perturbation theory (MP2). This combination of methods yields valuable structural and dynamical information beyond that delivered by the sum of its constituents and enables us to characterize the morphology on a molecular level and eventually to derive its relationships to macroscopic properties.

2. Supramolecular Assembly Probed by Solid-State NMR Spectroscopy

We characterized the supramolecular assembly of the $C_{8,7}$-PDI system by solid-state NMR spectroscopy (see the Supporting Information for details). While this technique cannot provide information about long-range ordering phenomena, it is very sensitive to the local environment of the probed nuclei. Specifically, the ^{1}H NMR chemical shift is known to be a highly sensitive probe of both hydrogen bonding and the $\pi-\pi$ packing of supramolecular assemblies.[18,19]

Figure 1b displays a 2D ^{1}H−^{13}C correlation spectrum of the $C_{8,7}$-PDI sample recorded using a short cross-polarization time (500 μs) to obtain information about directly bonded proton and carbon atoms as well as homonuclear ^{1}H−^{1}H decoupling to improve the spectral resolution of the ^{1}H dimension. An assignment of ^{1}H resonances to ^{13}C resonances was easily achieved for the aliphatic species (H_{br} and side chains) by using the contours of the 2D spectrum and the skyline projections for each dimension. However, the assignment of the aromatic protons H_{in} and H_{out} was less straightforward because these two signals have contours with a similar appearance in the 2D spectrum (Figure 1b) and show only a single correlation each. To clarify which assignment is correct, we took advantage of the results of the present ab initio NMR calculations (see below), which are summarized in Table 1. These show that the most shielded (or upfield-shifted) proton is H_{in}, independent of the local stacking arrangement of the $C_{8,7}$-PDI core used in the calculations. On this basis, the final assignment of ^{1}H resonances to ^{13}C resonances was achieved, as illustrated in Figure 1b using the dashed lines and employing the color scheme from Figure 1a.

Further information about the local molecular assembly of the $C_{8,7}$-PDI system can be obtained from ^{1}H double-quantum (DQ) MAS experiments, where through-space information regarding dipolar-coupled protons is acquired. The resulting spectra are shown in Figure 2a,b, where two different recoupling periods have been used for excitation and reconversion of DQ coherences. In Figure 2a, essentially all of the correlations between the resolved proton sites within a single PDI molecule are observed. However, the most striking feature of Figure 2a is the intense $H_{br}-H_{br}$ self-correlation peak located on the diagonal ($SQ_{iso} = 4.8$ ppm, $DQ_{iso} = 9.6$ ppm); this peak is even more pronounced in Figure 2b, where a longer DQ recoupling period was used. This correlation cannot be attributed to the antipodal H_{br} within a single PDI molecule, because the distance of ∼15 Å between H_{br} atoms is far beyond what can be observed with ^{1}H DQ MAS NMR techniques. Thus, the $H_{br}-H_{br}$ self-correlation peak in Figure 2a,b must originate from an intermolecular contact between two adjacent $C_{8,7}$-PDI molecules within the columnar stack.

The strong self-correlation peak between two adjacent $C_{8,7}$-PDI molecules can also be quantified in terms of a $^1H_{br}-^1H_{br}$ dipolar coupling constant D, which is inversely proportional to the cube of the internuclear distance ($D \propto 1/d^3_{br-br}$). This distance can be obtained experimentally by recording an additional ^{1}H DQ−SQ spectrum with a longer DQ recoupling time and a non-rotor-synchronized t_1 increment of less than one rotor period, thereby encoding the full DQ sideband pattern in the indirect dimension.[20] The resulting ^{1}H−^{1}H sideband pattern, shown in Figure 2(c), can be reproduced using an effective $H_{br}-H_{br}$ distance (d_{br-br}) of 3.7 ± 0.1 Å. This value correlates well with a $\pi-\pi$ packing arrangement of the $C_{8,7}$-PDI cores, assuming $\pi-\pi$ stacking distances ($d_{\pi-\pi}$) in the range 3.4−3.5 Å and a relative rotation of neighboring $C_{8,7}$-PDI molecules with respect to one another (α) of 25−40° (see Figure 3).[8] Larger pitch angles are not compatible with the observed DQ sideband pattern, since they would result in larger $H_{br}-H_{br}$ distances, which in turn would increase the intensity of the first-order sideband at the expense of the higher-order bands. It should be noted that the actual distance determined from the ^{1}H DQ sideband pattern in Figure 2c has to be considered as an effective distance averaged from an ensemble of adjacent $C_{8,7}$-PDI molecules.

3. Local Ordering from NMR Sideband Patterns

The mobilities of the perylene core region of $C_{8,7}$-PDI and the attached side chains were assessed by 2D ^{1}H−^{13}C rotor-

(17) Hoeben, F. J. M.; Jonkheijm, P.; Meijer, E. W.; Schenning, A. P. H. J. *Chem. Rev.* **2005**, *105*, 1491.
(18) Ochsenfeld, C.; Brown, S. P.; Schnell, I.; Gauss, J.; Spiess, H. W. *J. Am. Chem. Soc.* **2001**, *123*, 2597.
(19) Brown, S. P. *Prog. Nucl. Magn. Res.* **2007**, *50*, 199.
(20) Schnell, I.; Spiess, H. *J. Magn. Reson.* **2001**, *151*, 153.

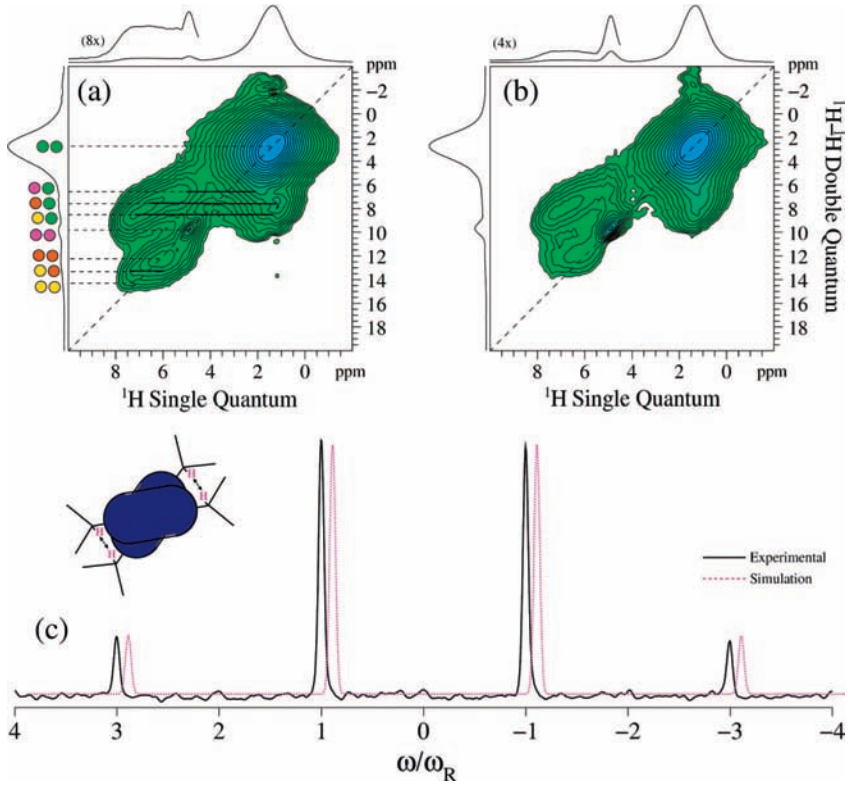

Figure 2. 2D rotor-synchronized ^{1}H DQ−SQ MAS NMR correlation spectra of $C_{8,7}$-PDI together with DQ and SQ skyline projections, recorded using a spinning frequency of 25.0 kHz and BaBa recoupling periods of (a) $1\tau_R$ and (b) $2\tau_R$. (c) Experimental DQ sideband pattern recorded with an $8\tau_R$ BaBa recoupling block and a spinning frequency of 25.0 kHz. The optimized simulation in (c) (dotted magenta curve) corresponds to a $H_{br}-H_{br}$ distance of 3.7 ± 0.1 Å and has been slightly shifted to the right for a better visual comparison with the experimental counterpart. The inset in (c) illustrates two $C_{8,7}$-PDI molecules within the columnar stack and the intermolecular distance encoded in the DQ sideband pattern. The assignment of resonances in (a) employs the color scheme of Figure 1a, and the numbers above the expansions (4.5−10.0 ppm) in (a) and (b) are vertical expansion factors relative to the full skyline projections. For experimental and simulation details, see the Supporting Information.

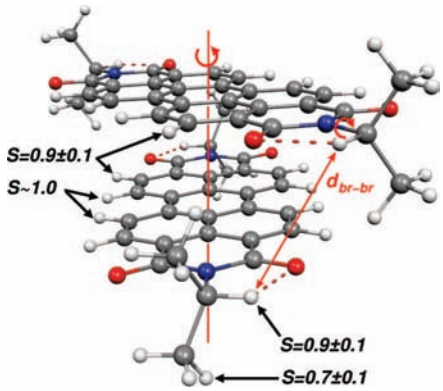

Figure 3. Illustration of the local arrangement between two successive $C_{8,7}$-PDI molecules (with side chains omitted), with order parameters (S) of selected hydrogens as obtained from NMR spinning sideband patterns via eq 1. The order parameter of the CH_3 group corresponds to the *terminal* methyl group of the actual $C_{8,7}$-PDI. Also indicated are the dihedral angles that determine the orientation of the side chains, the pitch angle between the successive perylene cores relative to the stack axis, and the $H_{br}-H_{br}$ distance d_{br-br}.

encoded solid-state NMR experiments in which ^{13}C-site-specific information about the effective ^{1}H−^{13}C heteronuclear dipolar couplings is detected.[21] The results from these experiments are shown in Figure 4, where experimental sideband patterns for each of the indicated ^{13}C sites are shown along with optimized simulations (see the Supporting Information for details) based on the dipolar couplings given next to each of these spectra. An estimate of the local ordering can be achieved by defining an effective order parameter S_{CH}^{NMR} given by

$$S_{CH}^{NMR} = \frac{D_{CH}^{eff}}{D_{CH}^{rigid}}, \qquad (1)$$

where the dipolar coupling constants D_{CH}^{rigid} for rigid CH and motion-averaged CH_3 groups are 21.0 and 6.9 kHz, respectively.[22] Using this equation yielded the effective order parameters given in Figure 3. The order parameters for the perylene-core part of $C_{8,7}$-PDI and the side-chain branching point are seen to be in the range 0.9−1.0, whereas the methyl end group has an order parameter of 0.7. These results clearly indicate that the perylene cores are quite rigid and neither fluctuate nor undergo any type of motion on the time scale of the NMR experiment. The slightly decreased value of 0.7 for the methyl end group of the side chains shows that the these are somewhat flexible and can move on the time scale of the NMR experiment. Both findings illustrate the low molecular mobility within the columnar $C_{8,7}$-PDI stacks.

4. Ab Initio NMR Signatures of Local Packing

In order to understand the effect of different neighbor orientations on the NMR spectra of columnar $C_{8,7}$-PDI stacks,

(21) Saalwächter, K.; Schnell, I. *Solid State NMR* **2002**, *22*, 154.

(22) Saalwächter, K. R.; Graf, H. S. *J. Magn. Reson.* **2001**, *148*, 398.

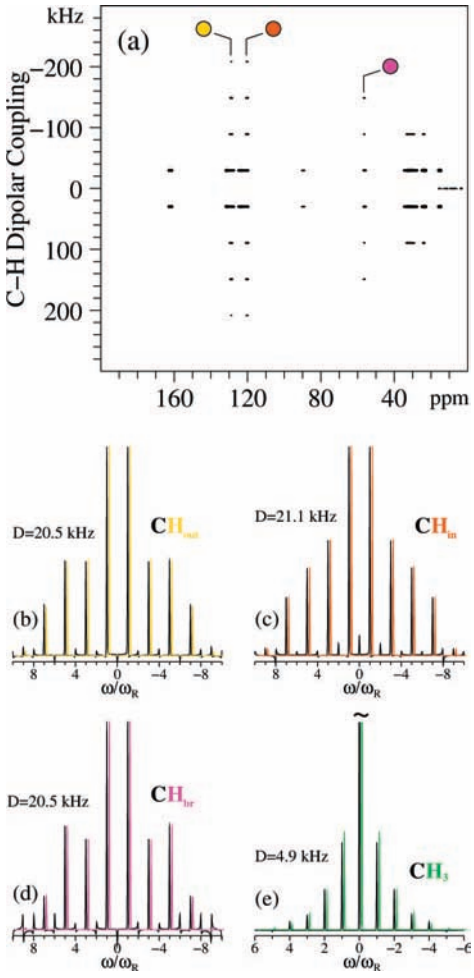

Figure 4. (a) 2D contour plot of the $^{1}H-^{13}C$ REPT-HDOR spectrum for the investigated $C_{8,7}$-PDI sample acquired using a recoupling time of $4\tau_R$ and a spinning frequency of 30.0 kHz. The black spectra shown in (b−d) are slices taken at the positions indicated in (a), whereas the spectrum in (e) was obtained from a 2D $^{1}H-^{13}C$ REREDOR spectrum recorded using a recoupling time of $3\tau_R$ for the REDOR pulse trains. The effective C−H dipolar couplings D determined from the slices in (b−e) are given, and the corresponding simulations are illustrated by the colored spectra in (b−e), which have been slightly shifted to the right for better comparison with their experimental counterparts (black). The dynamical order parameters calculated using eq 1 are given in Figure 3. The numerical errors are estimated to be ±0.2 kHz.

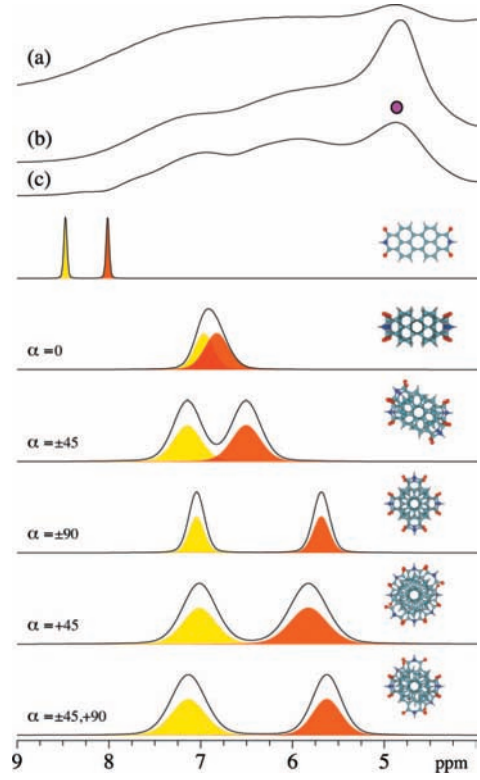

Figure 5. (top) (a) ^{1}H MAS NMR spectrum of $C_{8,7}$-PDI, (b) very fast ^{1}H MAS NMR spectrum, and (c) $^{1}H-^{1}H$ decoupled NMR spectrum recorded using a windowed PMLG-5 sequence during detection. All three spectra were obtained at 20.0 T using spinning frequencies of (a, c) 15.0 and (b) 50.0 kHz. It should be noted that very fast MAS (b) and stroboscopic detection with a lower spinning frequency (c) remove the contribution from homonuclear $^{1}H-^{1}H$ dipolar couplings to the same degree, leaving the spectra mainly influenced by packing effects, as investigated in this work. (bottom) Six calculated spectra summarizing the results from the ab initio NMR calculations for a single perylene monomer with different packing arrangements described by the stacking angle α. The color scheme of Figure 1 is used.

we built simplified model systems that represent several different local packing motifs (see the Supporting Information for details). Our models were designed for ab initio calculations under periodic boundary conditions, in which only a limited amount of disorder can be incorporated because of the high computational cost of such calculations. We assumed infinite stacks of coaxial PDIs with a common distance of 3.55 Å and different stacking angles α between successive molecules (also see the illustrations in Figure 5). While the simplest configuration consists of a zero pitch (α = 0° in Figure 5), α = ±45° means a forth-and-back arrangement of subsequent PDIs, and α = +45° corresponds to a quasi-helical structure with eight molecules per complete winding. Additionally, we built a stack with α = 90° and one with a combination of α = 45° and α = 90° increments. Thanks to the twofold symmetry of the PDIs, all of these models can be implemented by a periodic setup with four molecules per unit cell; we verified that using an appropriate unit cell with six molecules does not change the results. In addition, we neglected the side chains in our model systems, because in this section our focus is on the direct interactions of the aromatic and antiaromatic cores of the molecules with their neighbors.

Our aim was to predict the isotropic chemical shifts that the aromatic PDI protons would exhibit in our models as well as to quantify the degree of sensitivity of these resonances toward small fluctuations in the actual conformations. For this purpose, we used ab initio Car−Parrinello molecular dynamics (CPMD) simulations[23,24] at a temperature of $T \approx 200$ K; this permitted the incorporation of Brownian motion into our model, which otherwise would have been entirely static. We note, however, that the time scale that could be reached with our ab initio simulations was only on the order of picoseconds, while possible conformational fluctuations in the real system might have characteristic times of milliseconds or longer. Thus, our CPMD simulations, which furthermore were performed at a comparably low temperature, rather yielded a sampling of the *local* phase space point at which the system was initially prepared.

In order to learn about the spectroscopic signatures of the packing motifs represented by our models, we sampled the full trajectories with calculations of NMR resonances from 10 snapshots at random times within the trajectory. In addition to

(23) Car, R.; Parrinello, M. *Phys. Rev. Lett.* **1985**, *55*, 2471.
(24) Hutter, J.; Curioni, A. *ChemPhysChem* **2005**, *6*, 1788.

Table 1. Numerical Values of ab Initio ^{1}H NMR Chemical Shifts δ (ppm) of the Aromatic Inner and Outer Perylene Protons Using Different Pitch Angles α (deg), Along with Their Standard Deviations $\Delta\delta$ and $\Delta\Sigma$

α	$\langle\delta\rangle_{inner}$	$\langle\delta\rangle_{outer}$	$\Delta\delta_{inner}$	$\Delta\Sigma_{inner}$	$\Delta\delta_{outer}$	$\Delta\Sigma_{outer}$
0	6.92	7.05	0.97	0.31	0.66	0.26
±45	6.74	7.27	1.23	0.45	0.93	0.41
±90	5.81	7.17	0.75	0.22	0.70	0.24
+45	5.92	7.11	1.15	0.48	0.97	0.43
±45, +90	5.62	7.20	0.77	0.41	0.76	0.48
monomer	8.14	8.62				

the average chemical shifts of the four inner and four outer protons per perylene, we computed their standard deviations $\Delta\delta$ according to the equation

$$\Delta\delta^2 = \langle\delta_{(t,\mathrm{H})}{}^2\rangle_{t,\mathrm{H}} - \langle\delta_{(t,\mathrm{H})}\rangle_{t,\mathrm{H}}{}^2 \qquad (2)$$

where the averages are taken over all snapshots (indicated by the subscript *t*) and all chemically equivalent protons (subscript H). The standard deviation obtained via eq 2 gives one global value for the temporal fluctuations of the computed shifts of all of the protons of a given model during the CPMD simulation. This value (given in Table 1) can serve as an estimate of the statistical error from the ab initio sampling. We also computed the standard deviation of the time-averaged proton shifts with respect to each other, $\Delta\Sigma$, according to the equation

$$\Delta\Sigma^2 = \langle\langle\delta_{(t,\mathrm{H})}\rangle_t{}^2\rangle_{\mathrm{H}} - \langle\langle\delta_{(t,\mathrm{H})}\rangle_t\rangle_{\mathrm{H}}{}^2 \qquad (3)$$

In this way, it is possible to characterize the strength of the effect of small geometric fluctuations on the distribution of NMR chemical shifts. Although the line width of an experimental NMR resonance is determined (in part) by the distribution of morphologies in the actual sample, which is not directly related to the spread from eq 3, we can still use $\Delta\Sigma$ as an estimate (neglecting relaxation effects) of the broadness of the experimental line widths, which are shown in the top portion of Figure 5. Together with the averaged ab initio NMR chemical shift values, this yields the five patterns shown in the bottom portion of Figure 5, where the spreads from eq 3 have been used as the widths of Gaussian peaks centered at $\langle\delta_{(t,\mathrm{H})}\rangle_{t,\mathrm{H}}$.

In comparison with the experimental spectrum in Figure 5, the first observation from the computed patterns is that there is indeed a noticeable packing effect on the position of the NMR chemical shift lines for the aromatic protons. A clear low-frequency displacement is observed for all of the PDI stacks. While $\alpha = 0°$ yields overlapping shifts, which are clearly incompatible with the experimental spectrum (upper plots in Figure 5), all of the other stacking angles fit the partially resolved experimental line shape.

An interesting feature concerns the computed spreads of the chemical shifts in our model systems, which represent the variability of the NMR signal due to geometric fluctuations in the stack (with respect to both the stacking angle and the inter-PDI distance). While the $\alpha = 90°$ configuration shows very low flexibility, corresponding to a narrow line, the spread increases for the $\alpha = +45°$ and $\alpha = \pm45°$ cases and becomes very large for the most disordered systems, such as could be envisioned from a combination of $\alpha = 45°$ and $\alpha = 90°$ pitches.

These findings show that when the relative stacking angles are small, the proton NMR lines react quite sensitively to variations in the morphology, which naturally occur in any real sample that has no long-range crystalline order. In turn, in the $\alpha = 90°$ arrangement, the packing effects are present but insensitive to these geometric fluctuations. The physical reason for this observation can be derived from the nucleus-independent chemical shift (NICS) map of PDI (Figure 6).[29,30,31] The magnetic shielding of a PDI molecule has strong gradients right atop the six-membered aromatic rings, which is where the protons of the neighboring PDIs are located when the stacking angle is $\alpha = 45°$. In the $\alpha = 90°$ case, however, the neighboring protons are found in regions that do not exhibit such strong gradients, and hence, the through-space shielding does not vary as much when the PDIs move relative to each other.

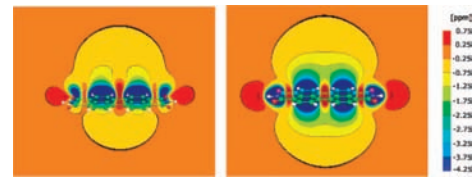

Figure 6. Two slices of the NICS map of the PDI molecule, illustrating the magnetic shielding that a given PDI exerts on its immediate spatial environment.

In summary, the NMR chemical shift fingerprints obtained from first-principles calculations of periodic stacks indicate that the most likely stacking angles are $\alpha \approx 45°$. In contrast to this, the more symmetric $\alpha \approx 0°$ and $\alpha \approx 90°$ conformations are less consistent with the experimental line shape. The difference between a truly helical structure ($\alpha = +45°$) and its alternating analogue ($\alpha = \pm45°$), however, cannot be resolved.

5. Side-Chain Orientation from ab Initio Calculations

In order to determine a preferential orientation of the alkane side chains, we computed the energy change as a function of the dihedral N−C angle (as indicated in Figure 3) in a single isolated molecule in which the aliphatic side chains of $C_{8,7}$-PDI were replaced with a single methyl group. In the optimized geometry of the molecule, there is a weak intramolecular CH···O hydrogen bond (also sketched in Figure 3), and the methyl groups point out of the plane of the PDI core. When the side chain is rotated by 90° around the N−C bond indicated in the figure, the CH···O hydrogen bond is broken, and there is a significant steric repulsion between the methyl group and the oxygen atom. In our ab initio calculations at the DFT level of theory, this is reflected by an energy increase of ∼44 kJ/mol upon the 90° rotation. This energy is about twice as large as what would be expected from a regular OH···O hydrogen bond. Hence, the CH···O bond can be considered as quite stable, forcing the side chains into the conformation suggested in Figure 3. It is noteworthy that the existence of a weak intramolecular CH···O hydrogen bond is also confirmed by the experimental ^{1}H NMR chemical shift of the corresponding proton. The value of 4.8 ppm (pink code in Figure 1) is considerably deshielded compared with the commonly expected aliphatic region of 0−3 ppm (green code in Figure 1).

6. Angular Energy Surface of the $C_{8,7}$-PDI Dimer

Intuitively, the steric repulsion between the aliphatic chains of adjacent $C_{8,7}$-PDI molecules confines the pitch angles between the molecules in the stack to values greater than 30°. Also, at smaller pitch angles than illustrated in Figure 3, the methyl group (representing the CH_2 chains) is too close to the oxygen atoms of the neighboring $C_{8,7}$-PDI.

In order to understand the potential energy surface for $C_{8,7}$-PDI more quantitatively, we computed the packing interactions

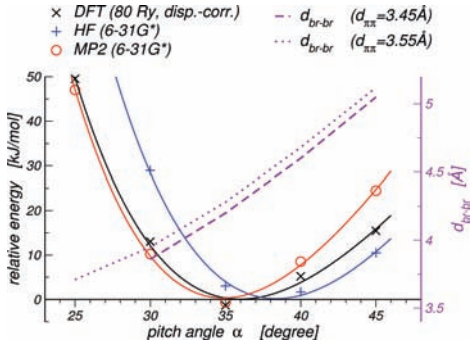

Figure 7. Variation of the $\pi-\pi$ stacking energy of the dimeric $C_{8,7}$-PDI model system (illustrated in Figure 3) as a function of the pitch angle at the HF, MP2, and DC-DFT levels of theory (the solid lines are fits to Morse-type potentials). Also shown is the pitch-angle dependence of the distance d_{br-br} between H_{br} protons on adjacent PDI molecules (dashed and dotted violet lines; $d_{\pi-\pi}$ denotes the stacking distance between the PDI cores).

in the isolated dimer model (Figure 3; see the Supporting Information for details) at discrete pitch angles between 30 and 45° at both the explicitly correlated MP2 and dispersion-corrected DFT (DC-DFT) levels of theory.[25,26,32] The results are shown in Figure 7, where all of the energies are given relative to the respective minimum values, and a stacking distance of $d_{\pi-\pi}$ =3.55 Å was used. While a Hartree−Fock (HF) calculation predicts an energy minimum at a pitch angle of 39°, the energy curves at both the MP2 and DC-DFT levels of theory indicate an equilibrium angle of $\alpha \approx 35°$.

This energy minimum is in good agreement with the local motifs obtained from the analysis of the NMR spectroscopic fingerprints presented in the previous sections. The arrangement corresponds to a distance between adjacent H_{br} protons of ∼4 Å, which is somewhat larger than but still in good agreement with the value obtained from the NMR sideband patterns (Figure 2). Especially with the use of slightly smaller stacking distances (e.g., $d_{\pi-\pi}$ = 3.45 rather than 3.55 Å), the H_{br} protons automatically acquire a shorter distance. Analogous MP2 and DC-DFT calculations for $d_{\pi-\pi}$ =3.45 Å predict precisely the same pitch angle of $\alpha = 35°$ at the energy minimum (data not shown). This data is in good agreement with recently published values for a PDI dimer without any side chains, where an angle of $\alpha = 30°$ was found for the ground-state conformation.[27]

While the pitch angles obtained from solid-state NMR experiments and electronic structure calculations are in good mutual agreement, they do not provide evidence for a truly helical structure of the $C_{8,7}$-PDI stack with a four- or five-layer periodicity, as has been postulated in previous work based on wide-angle X-ray scattering (WAXS) measurements.[8] Instead, our results suggest an alternative interpretation of the meridional WAXS reflection corresponding to a distance of 1.26 nm. Such a value would be compatible with the lateral distance between $C_{8,7}$-PDI columns with an ellipsoidal base area that are arranged with their flat sides facing each other. The separation of 1.26 nm would still permit enough space between the anisotropic $C_{8,7}$-PDI stacks for a single polyethylene chain, since the lateral extension of the PDI core is no more than 9 Å.

7. Conclusion

In this work, we have derived detailed aspects of local packing motifs of $C_{8,7}$-PDI stacks from their spectroscopic fingerprints obtained by combining solid-state NMR experiments with ab initio calculations and first-principles molecular dynamics simulations. The competition between the $\pi-\pi$ dispersion forces on one hand and steric factors as well as an intramolecular CH···O hydrogen bond on the other hand lead to a relative pitch angle between adjacent molecules of 30−45°. At intermolecular pitch angles in this range, the magnetic shielding of neighboring $C_{8,7}$-PDI molecules yields a characteristic pattern in the NMR chemical shifts predicted from ab initio calculations that is compatible with the corresponding NMR line shape. The order parameters obtained from NMR sideband patterns further confirm that the core of the $C_{8,7}$-PDI stack is essentially rigid and shows no signs of liquid-crystalline motion.

This local packing morphology is closely related to the macroscopic properties of $C_{8,7}$-PDI wires. In particular, ongoing studies within a concerted research effort have shown that the shape of the pitch angle distribution directly controls their electronic conductivity.[16] A complementary investigation has shown that the choice of the specific side chain that is attached to the $C_{8,7}$-PDI cores critically determines the pitch angle distribution.[28]

Thus, our approach provides a general route for understanding the formation of supramolecular stacks with a controlled packing architecture and elucidating their relationship to microscopic packing features. It is applicable to supramolecular assemblies, even if these exhibit only a small amount of long-range order as required for accurate X-ray scattering experiments. Such rationally designed columnar stacks are crucial building blocks for the emerging field of molecular electronics.

Acknowledgment. We thank Zihong Liu for providing the $C_{8,7}$-PDI sample and W. Pisula, D. Andrienko, and V. Marcon for valuable discussions. M.R.H. thanks the Carlsberg Foundation for financial support in the form of a Research Fellowship. This work was partially supported by the Deutsche Forschungsgemeinschaft under Grants SE1008/5 and SE1008/6.

Supporting Information Available: Additional information about experimental and computational details. This material is available free of charge via the Internet at http://pubs.acs.org/.

JA8095703

(25) Møller, C.; Plesset, M. S. *Phys. Rev.* **1934**, *46*, 618.
(26) von Lilienfeld-Toal, A.; Tavernelli, I.; Rothlisberger, U.; Sebastiani, D. *Phys. Rev. Lett.* **2004**, *93*, 153004.
(27) Fink, R. F.; Seibt, J.; Engel, V.; Renz, M.; Kaupp, M.; Lochbrunner, S.; Zhao, H.-M.; Pfister, J.; Würthner, F.; Engels, B. *J. Am. Chem. Soc.* **2008**, *130*, 12858.
(28) Hansen, M. R.; Schnitzler, T.; Pisula, W.; Graf, R.; Müllen, K.; Spiess, H. W. *Angew. Chem., Int. Ed.* **2009**, in press.
(29) Schleyer, P. v. R.; Maerker, C.; Dransfield, A.; Jiao, H.; Hommes, N. J. R. v. E. *J. Am. Chem. Soc.* **1996**, *118*, 6317.
(30) Sebastiani, D. *ChemPhysChem* **2006**, *7*, 164.
(31) Sebastiani, D.; Kudin, K. *ACS Nano* **2008**, *2*, 661.
(32) Møller, C.; Plesset, M. S. *Phys. Rev.* **1934**, *46*, 618.